

## Research Article

# On Positioning and Vibration Control Application to Robotic Manipulators with a Nonideal Load Carrying

Jeferson J. Lima,<sup>1</sup> José M. Balthazar <sup>1,2</sup> Rodrigo T. Rocha <sup>2</sup> Frederic C. Janzen,<sup>2</sup> Davide Bernardini,<sup>3</sup> Grzegorz Litak <sup>4,5</sup> Dailhane G. Bassinello <sup>1,6</sup> and Angelo M. Tusset <sup>2</sup>

<sup>1</sup>São Paulo State University, Faculty of Engineering of Bauru, 17033-360 Bauru, SP, Brazil

<sup>2</sup>Federal University of Technology-Parana, Department of Electronics, 84016-210 Ponta Grossa, PR, Brazil

<sup>3</sup>Sapienza Università di Roma, Roma, Italy

<sup>4</sup>Faculty of Mechanical Engineering, Lublin University of Technology, Nadbystrzycka 36, PL-20-618 Lublin, Poland

<sup>5</sup>Department of Process Control, AGH University of Science and Technology, Mickiewicz Alley 30, 30-059 Krakow, Poland

<sup>6</sup>Federal Institute of Paraná, Campo Largo, Paraná, Brazil

Correspondence should be addressed to Angelo M. Tusset; [tusset@utfpr.edu.br](mailto:tusset@utfpr.edu.br)

Received 12 July 2018; Revised 20 December 2018; Accepted 27 December 2018; Published 14 February 2019

Academic Editor: Davood Younesian

Copyright © 2019 Jeferson J. Lima et al. This is an open access article distributed under the Creative Commons Attribution License, which permits unrestricted use, distribution, and reproduction in any medium, provided the original work is properly cited.

In recent years, the evolution of artificial intelligence techniques has widely grown such that it gives new ways to improve human life, not only at work but also living. Nowadays, to the human being, physical human-robot interactions (PHRIs) have been presented very important and present itself as a major challenge for the current engineering. Therefore, this work designs and analyses a two-degree-of-freedom robotic arm with flexible joints driven by a DC motor. Due to the interaction between the robot links and flexible joints, the arm may present overshoots when it is moved such that it becomes difficult to manipulate the arm. Therefore, Magnetorheological dampers (MR damper or MR brake) are attached to the links of the arm in order to control such overshoot and provide a way to adjust the mechanical limitations of the arm. The dynamics of the system will be investigated, showing the appearance of chaotic behavior due to the coupling of the manipulator to the motors. After that, the feedback control is obtained through the state-dependent Riccati equation (SDRE) aiming the control of the positioning of the manipulator and the torque applied on the MR damper. Numerical results showed that the proposed control using hybrid actuators, DC motor, and MR brake was effective to control the position and behavior of the flexible joints of the manipulators.

## 1. Introduction

Although in recent years, the human interaction with intelligent systems, such as voice or video recognition devices, has grown exponentially due to the evolution of artificial intelligence techniques, physical human-robot interaction (PHRI) presents itself as a major challenge for current engineering. Nowadays, the fact that an industrial that works only with robots is not feasible, much less the industry that works only with human workers in activities that cause the degradation of health. Therefore, a model of integration,

physical, and cognitive logic between devices and people sharing the workspace is very important.

PHRIs have being designed to coexist and collaborate with operators in handling, assembling, cutting, and other tasks, without presenting a risk in this interaction [1–6].

There are several attempts to ensure the safety of humans within a workspace shared with machines. A large number of research studies have focused on the development of manipulators that are intrinsically safe. That is, manipulators in which can guarantee some level of collision safety in the absence of a controller through their mechanical properties.

In particular, vibrations which appear during the positioning of the robotic arm should be controlled to improve safety PHRI, which is also important for increasing efficiency and operation precision.

Many researchers have concentrated their efforts to study about manipulators with flexible links due to their advantage related to rigid ones. Such advantages include faster response, lower energy consumption, smaller actuators, less overall mass, and in general, smaller final cost [7–9]. Due to its natural flexibility, control of these systems takes into account both rigid body and elastic degree of freedom, so that their mathematical models have to consider the interactions between the actuators and load to be handled.

Therefore, to improve the efficiency of using the manipulators, control strategies are required. The SDRE control is being applied in many nonlinear systems due to its easy application and advantage of considering the influence of nonlinearities of the system, i.e., there is no need to linearize the system to be applied [10–14]. Such control has been widely used in rigid and flexible robotic manipulators as the works of authors [8, 14–23].

In addition, the links of the manipulators generally are driven by a DC motor; however, another kind of actuator which has demonstrated to be a good alternative to suppress vibrations or even be used as a drive device is the magnetorheological (MR) brake. According to [1, 24], the MR device consists of a MR fluid composed of micro-sized magnetic particles, located inside a liquid carrier, which forms chain-like structure when an external magnetic field is applied, resulting in an increase of the apparent viscosity of the fluid. The MR actuator is usually used as a damper and may be used as a passive or semiactive actuator.

In [25], the authors demonstrated the efficiency of the application of the magnetorheological (MR) brake in the positioning control of the two-degree-of-freedom robotic arm designed with flexible joints. The considered control is composed of two controls: a feedforward and a feedback by using the SDRE, and the torque of the MR damper is modelled by means of a neural network.

The present paper is a continuation of the previous developments [25]; however, the modelling of the MR damper is performed by the use of the explicit mathematical model. In this way, this work considers the positioning control of the dynamical behavior of a robot manipulator arm with flexible joints driven by a DC motor and MR brake, controlled for a feedback control obtained by the SDRE control, and considering a nonideal load carrying, and the control of the chaotic behavior. The MR brake torque is modelled by considering the behavior of a Bingham fluid. The main objective here is to study and control of the dynamics of a robot manipulator arm with flexible joints driven by a DC motor and MR brake, controlled by the SDRE control. The main contribution and new approach of this work is the inclusion of the flexible cables, and a new degree of freedom was included to the force on the load.

The study of vibrations in robot arms is of utmost importance. Robot arms are used for manipulations of objects, tools, and even for surgical purposes, and sometimes, vibrations are not allowed due to the needed precision in the

manipulation operation. Then, the investigation and control of such vibrations become very important to robot arms.

This work is organized as follows: first section is the introduction; second and third sections discuss the dynamics of the manipulator with the modelling of the system and dynamical analysis through Poincaré maps and Lyapunov's exponent analysis; fourth section shows the control proposal and development; fifth section shows the use of MR brake with the DC motor to control the system; and last section is the conclusions of this work.

## 2. Dynamics of the Manipulator with Flexible Joint

The dynamics of a robot manipulator is composed typically by an open kinematic chain, where each segment of their links, being rigid or flexible, has links from the base to the extreme of the actuator. In this way, the positioning and orientation of the coordinate system of the manipulator are defined by a universal coordinate system, which is considered as a Cartesian plane coordinate system.

A vector position  ${}^A\mathbf{P}$  is established as a  $\mathfrak{R}^{3 \times 1}$  (3-dimension) vector to define the motions of the robotic arm at  $X$ ,  $Y$ , and  $Z$  coordinates in a plane  $\{A\}$ . The individual elements of  ${}^A\mathbf{P}$  are defined by

$${}^A\mathbf{P} = \begin{bmatrix} p_x \\ p_y \\ p_z \end{bmatrix}. \quad (1)$$

The graphical representation of the vector position is illustrated in Figure 1.

In addition, the vector position can be rotated by a matrix rotation represented by  $\mathbf{R}$  in the following equation:

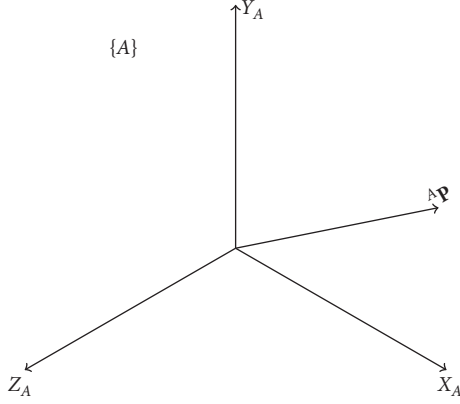
$${}^B\mathbf{R} = \begin{bmatrix} r_{11} & r_{12} & r_{13} \\ r_{21} & r_{22} & r_{23} \\ r_{31} & r_{32} & r_{33} \end{bmatrix}. \quad (2)$$

As the plane of reference  $\{A\}$  does not coincide with any other coordinates in a plane  $\{B\}$ , the displacements between such planes are called translation given by the vector  $\mathbf{D}_A$ , where  ${}^A\mathbf{Q}$  represents the translation between  $\{A\}$  and  $\{B\}$  planes, whose vectors are expressed in the following equation:

$${}^A\mathbf{Q} = \begin{bmatrix} q_x \\ q_y \\ q_z \end{bmatrix}, \quad (3)$$

$${}^B\mathbf{D} = \begin{bmatrix} 1 & 0 & 0 & q_x \\ 0 & 1 & 0 & q_y \\ 0 & 0 & 1 & q_z \\ 0 & 0 & 0 & 1 \end{bmatrix}.$$

Therefore, the translation of the coordinates can be expressed in a new notation with both translation and rotation of a vector, according to equation (4), where the matrix  $\mathbf{D}_A$  is incorporated in the new notation.

FIGURE 1: Vector related to the plane  $\{A\}$ .

$$\begin{bmatrix} {}^B \mathbf{P} \\ {}^A \mathbf{P} \\ 1 \end{bmatrix} = \underbrace{\begin{bmatrix} {}^A \mathbf{R} & {}^A \mathbf{Q} \\ 0 & 0 & 0 & 1 \end{bmatrix}}_{{}^A \mathcal{A}} \begin{bmatrix} {}^B \mathbf{P} \\ 1 \end{bmatrix}. \quad (4)$$

In equation (4), the matrix  ${}^A \mathcal{A}$  represents the homogeneous transformation matrix, in this case, composed of the rotation matrix  ${}^A \mathbf{R}$  and the translation matrix  ${}^A \mathbf{Q}$ . The result of the operation of equation (4) is graphically represented by Figure 2.

In the generalized form, the homogeneous transformation  ${}^i T$  can be expressed by successive rotations and translations and can be found by calculating the product of the successive transformations of  ${}^{i-1} \mathcal{A}_i$ , as given by

$$\begin{aligned} {}^i T &= {}^0 \mathcal{A}_1 \mathcal{A}_2 \dots \mathcal{A}_i = \prod_{j=1}^i {}^{j-1} \mathcal{A}_j, \quad i = 1, 2, \dots, n \\ &= \begin{bmatrix} x_i & y_i & z_i & p_i \\ 0 & 0 & 0 & 1 \end{bmatrix} = \begin{bmatrix} {}^i R & {}^i \mathcal{P} \\ 0 & 1 \end{bmatrix}, \end{aligned} \quad (5)$$

where  ${}^i \mathcal{P}$  is the orientation vector of the  $i$  reference related to the base 0.

The model of the manipulator with flexible joints with a load, illustrated in Figure 3, consists of two rigid links,  $l_1$  and  $l_2$ , and two flexible joints with  $k_s$  flexibility coefficient. The load of the manipulator is represented by a nonideal coupling of the cable flexibility, which is represented by  $k_c$ .

The flexibility behavior of the manipulator between the DC motor  $\theta_M = [\theta_4 \ \theta_5]^T$  and the link of the system  $\theta_M = [\theta_1 \ \theta_2]^T$  is given by the components of flexibility between the motor and the motor reduction box or even the motor axis. In addition, the magnetorheological dampers MR<sub>1</sub> and MR<sub>2</sub> are coupled in the joints of the robotic arm, where they will act to control the movement of the arms.

The manipulator model is modelled through the energy method of Lagrange, which uses the function of Lagrange, which is based on kinetic and potential energies, and Euler-Lagrange equation.

The kinetic energy  $\mathcal{T}$  is defined by the motion of the links of the manipulator, as given by

$$T = \frac{1}{2} m_{10} \dot{\mathbf{P}}_0^T \dot{\mathbf{P}}_0 + \frac{1}{2} m_{10} \dot{\mathbf{P}}_0^T \dot{\mathbf{P}}_0 + \frac{1}{2} m_{10} \dot{\mathbf{P}}_0^T \dot{\mathbf{P}}_0, \quad (6)$$

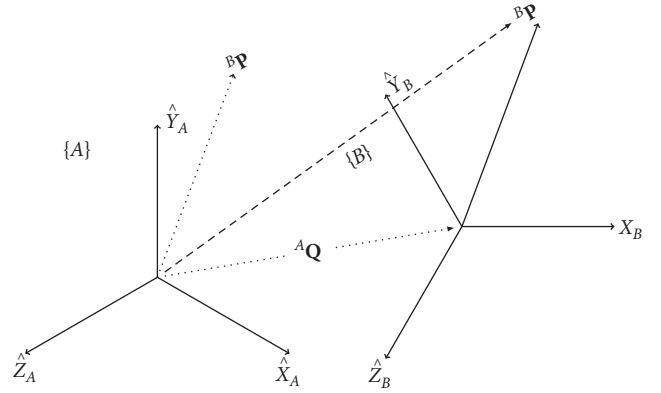
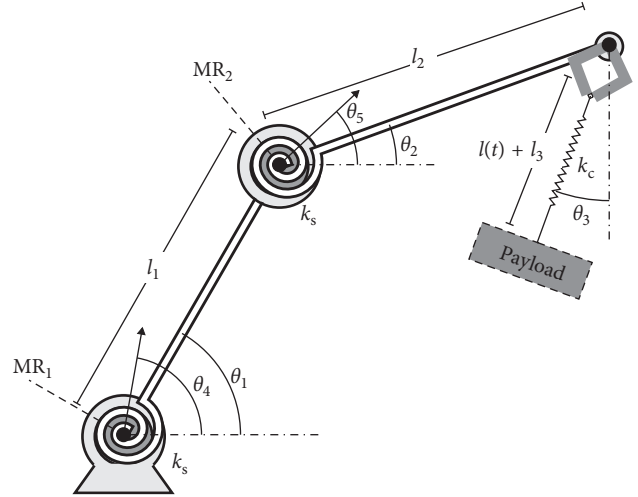
FIGURE 2: Homogenous transformation of the point  ${}^A \mathbf{P}$  by the rotation and translation operators.

FIGURE 3: Manipulator model with flexible joints, load, and magnetorheological breaks coupled to the joints.

where the load coupling equation to the handler is given by  $\ell(t) + l_3$  representing the coupling with flexible cargo characteristics.

The kinetic energy in terms of the generalized coordinates  $\theta_i$ , where  $i = [1, 5]$ , of the manipulator model, by introducing the matrices  $\mathcal{P}$  in equation (6), is given by the following equation:

$$\begin{aligned} \mathcal{T} &= \dot{\theta}_1 \dot{\theta}_2 l_1 l_2 (m_2 + m_3) \cos(\alpha) + \dot{\theta}_1 \dot{\theta}_3 l_1 m_3 (l_3 - \ell(t)) \cos(\beta) \\ &\quad + \dot{\theta}_2 \dot{\theta}_3 l_2 m_3 (l_3 - \ell(t)) \cos(\delta) + \dot{\theta}_1 l_1 m_3 \sin(\beta) \\ &\quad + \dot{\ell}(t) \dot{\theta}_2 l_2 m_3 \sin(\delta) + \frac{1}{2} l_1^2 (m_1 + m_2 + m_3) \dot{\theta}_1^2 \\ &\quad + \frac{1}{2} l_2^2 (m_2 + m_3) \dot{\theta}_2^2 + \frac{1}{2} m_3 \left( (l_3 - \ell(t))^2 \dot{\theta}_3^2 + \dot{d}_2^2 \right), \end{aligned} \quad (7)$$

where  $\alpha = \theta_1 - \theta_2$ ,  $\beta = \theta_1 - \theta_3$ , and  $\delta = \theta_2 - \theta_3$ .

The interaction between the engine and the handler presents nonoptimal characteristic, expressed by the spring component  $k_s$ ; hence, the potential energy is given by the

gravity force acting on each link and the torsional stiffness of each link, denoted by the following equation:

$$\mathcal{V} = \frac{1}{2}k_s(\theta_4 - \theta_1)^2 + \frac{1}{2}k_s(\theta_5 - \theta_2)^2 + m_1g_0^1\mathcal{P}_y + m_2g_0^2\mathcal{P}_y + m_3g_0^3\mathcal{P}_y, \quad (8)$$

Introducing the matrices  $\mathcal{P}$ , the full equation of potential energy  $\mathcal{V}$  becomes

$$\begin{aligned} \mathcal{V} = & l_1g(m_1 + m_2 + m_3)\sin(\theta_1) + l_2g(m_2 + m_3)\sin(\theta_2) \\ & - m_3g(\ell(t) - l_3)\sin(\theta_3) \\ & + \frac{1}{2}(k_s\theta_1^2 + k_s\theta_2^2 + k_c\ell^2 + k_s(\theta_4^2 + \theta_5^2)) \\ & - k_s\theta_1\theta_4 - k_s\theta_2\theta_5. \end{aligned} \quad (9)$$

Given kinetic and potential energies, Lagrange's function is defined, and Euler-Lagrange equation is applied to find the equations of motion of the system, considering the derivation of the coordinates as given by the following equation:

$$\begin{cases} \frac{d}{dt} \left( \frac{\partial \mathcal{L}}{\partial \dot{\theta}_i} \right) - \frac{d\mathcal{L}}{d\theta_i} = 0, \\ \frac{d}{dt} \left( \frac{\partial \mathcal{L}}{\partial \dot{\ell}} \right) - \frac{d\mathcal{L}}{d\ell} = 0, \end{cases} \quad (10)$$

where generalized coordinates are in function of  $\theta_i$  and the nonideal coupling  $\ell$ .

The equations of motion of the system can be expressed in the matrix form, denoted by the following equation:

$$\mathbf{M}(\theta, \ell) \begin{Bmatrix} \ddot{\theta} \\ \ddot{\ell} \end{Bmatrix} + \mathbf{C}(\dot{\theta}, \dot{\ell}, \theta, \ell) \begin{Bmatrix} \dot{\theta} \\ \dot{\ell} \end{Bmatrix} + \mathbf{K}(\theta, \ell) \begin{Bmatrix} \theta \\ \ell \end{Bmatrix} + \mathbf{G}(\theta) = 0, \quad (11)$$

where the matrices  $\mathbf{M}$ ,  $\mathbf{C}$ , and  $\mathbf{K}$  are

$$\begin{aligned} \mathbf{M} &= \begin{bmatrix} M_{11} & M_{21} & M_{31} & M_{41} \\ M_{12} & M_{22} & M_{32} & M_{42} \\ M_{13} & M_{23} & M_{33} & 0 \\ M_{14} & M_{24} & 0 & m_3 \end{bmatrix}, \\ \mathbf{C} &= \begin{bmatrix} 0 & C_{21} & C_{31} & 0 \\ C_{12} & 0 & C_{32} & 0 \\ C_{13} & C_{23} & C_{33} & 0 \\ C_{14} & C_{24} & C_{34} & 0 \end{bmatrix}, \\ \mathbf{K} &= \begin{bmatrix} k_s & 0 & 0 & 0 \\ 0 & k_s & 0 & 0 \\ 0 & 0 & 0 & -m_3g \sin \theta_3 \\ 0 & 0 & 0 & k_c \end{bmatrix}, \end{aligned} \quad (12)$$

where  $M_{11} = l_1^2(m_1 + m_2 + m_3)$ ,  $M_{21} = M_{12}$ ,  $M_{31} = l_1m_3(\ell - l_3)\sin(\theta_1 - \theta_2)$ ,  $M_{12} = l_1l_2(m_2 + m_3)\cos(\theta_1 - \theta_2)$ ,

$M_{22} = l_2^2(m_2 + m_3)$ ,  $M_{32} = M_{23}$ ,  $M_{13} = l_1m_3(\ell - l_3)\sin(\theta_1 - \theta_3)$ ,  $M_{23} = l_2m_3(\ell - l_3)\sin(\theta_2 - \theta_3)$ ,  $M_{33} = m_3(l_3 - \ell)^2$ ,  $M_{14} = l_1m_3\cos(\theta_1 - \theta_3)$ ,  $M_{24} = l_2m_3\cos(\theta_2 - \theta_3)$ ,  $M_{41} = l_1m_3\cos(\theta_1 - \theta_3)$ ,  $M_{42} = l_2m_3\cos(\theta_2 - \theta_3)$ ,  $C_{12} = -l_1l_2\theta_1\sin(\theta_1 - \theta_2)$ ,  $C_{13} = l_1m_3\theta_1(\ell - l_3)\cos(\theta_1 - \theta_3)$ ,  $C_{14} = -l_1m_3\theta_1\sin(\theta_1 - \theta_3)$ ,  $C_{21} = l_1l_2(m_2 + m_3)\sin(\theta_1 - \theta_2)$ ,  $C_{23} = l_2m_3\theta_2(\ell - l_3)\cos(\theta_2 - \theta_3)$ ,  $C_{24} = -l_2m_3\theta_2\sin(\theta_2 - \theta_3)$ ,  $C_{31} = l_1m_3(\theta_3 + 2(l_3 - \ell)\cos(\theta_1 - \theta_3) + 2\ell\sin(\theta_1 - \theta_3))$ ,  $C_{32} = l_2m_3(\theta_3 + 2(l_3 - \ell)\cos(\theta_2 - \theta_3) + 2\ell\sin(\theta_2 - \theta_3))$ ,  $C_{33} = -2m_3\ell(l_3 - \ell)^2$ ,  $C_{34} = m_3\theta_3(l_3 - \ell)$ .

The mechanical equations of the DC motor are described as in [5], denoted by equation (13). To the DC motor model, the flexible torque component is added; hence, the equation of motion of the motor coupled to the manipulator can be denoted by the following equation:

$$\ddot{\theta}_M = J_M^{-1}\{k_t i - b_v \omega - \tau_s(\theta, \theta_M)\}, \quad (13)$$

where the electric part of the DC motor is given by the following equation:

$$\frac{d}{dt} i = L_a^{-1}\{-R_a i - k_b \omega + v\}. \quad (14)$$

For a better relation between torque and velocity, the motors have an engine reduction box; the schematic of the reduction box model is illustrated in Figure 4, where  $J_L$  is the inertia of the link [5].

The relation constant between the magnitudes of the system is defined by the following equation:

$$\kappa = \frac{N_2}{N_1}. \quad (15)$$

Thus, it is explicit that the velocity ratio of the system is given by  $J_M = \kappa J_L$ . The viscous friction constant and inertia of the DC motor with the reduction box can be expressed by equation (16), considering the reflection effect of the variables by the ratio of the gears  $N_1$  and  $N_2$  [5]:

$$\begin{cases} J_{\text{eq}} = \kappa^2 J_L + J_M, \\ b = \kappa^2 b_{vL} + b_{vM}. \end{cases} \quad (16)$$

Therefore, the equations of motion of the system with mechanical and electrical parts of the DC motor coupled to the manipulator are given by the following equation:

$$\mathbf{M}(\theta, \ell) \begin{Bmatrix} \ddot{\theta} \\ \ddot{\ell} \\ \ddot{\theta}_M \\ \ddot{i}_M \end{Bmatrix} + \mathbf{C}(\dot{\theta}, \dot{\ell}, \theta, \ell) \begin{Bmatrix} \dot{\theta} \\ \dot{\ell} \\ \dot{\theta}_M \\ \dot{i}_M \end{Bmatrix} + \mathbf{K}(\theta, \ell, \theta_M, i_M) + \mathbf{G}(\theta) = 0. \quad (17)$$

To demonstrate the interaction between the subsystems, manipulator, and tool or load, the energy exchange between each element will be analysed. For the first model of the manipulator with nonideal load, it is intended here to analyse the interaction between the manipulator and the coupled load, where the motor axis is  $\theta_M = [\theta_4 \ \theta_5]^T$  at an arbitrary position such as  $\theta_4 = 1.2$  rad and  $\theta_5 = -1.2$  rad.

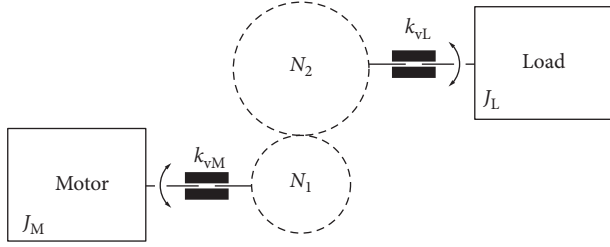


FIGURE 4: Schematic of the motor and load connected by a reduction box.

To obtain the steady-state energy of the model, it is considered  $\dot{\theta}_i = \dot{\theta} = 0$ , where the steady-state energy is given by  $\mathcal{E}_0^*$ . A small perturbation will be added in the system to analyse the interaction between the manipulator and load; thus,  $\mathcal{E} = \mathcal{E}_0^* + \zeta$ , where  $\zeta$  is a small fraction of  $\mathcal{E}_0^*$ . Based on  $\mathcal{E}$ , the initial conditions to analyse the interaction between the systems can be obtained.

The kinetic energy exchange between manipulator and load is shown in Figure 5. The kinetic energy of the manipulator is shown in red and kinetic energy of the cargo/load in black. It is observed that to the increase of energy of the load entails in the reduction of the energy of the manipulator, this event is given by the exchange of energy between the systems, in addition, showing the nonideality of the system.

The nonideal coupling characteristic, which for the first example of the manipulator is presented by the coefficient of elasticity of the element connecting the load to the manipulator, brings a new dynamics to the system in comparison to the ideal system.

### 3. Dynamical Analysis

The dynamic analyses of the system and all the numerical simulations, which will be carried out in this work, considered the parameters of Table 1. Such analyses will consider the use of tools such as Poincaré maps, phase planes, and Lyapunov exponent analysis.

The dynamical analysis consists of the interaction of links with the axes where the DC motor is coupled. Therefore, the axes  $\theta_M = [\theta_4 \ \theta_5]^T$  are fixed, and arbitrary is chosen with an initial condition of  $\theta_4 = 1.2$  rad and  $\theta_5 = -1.2$  rad.

Table 1 shows the whole nomenclature of the manipulator system and control strategy, which will be developed in the next section.

Figure 6 displays the phase plane of the two manipulators links  $\theta_1$  and  $\theta_2$ , with their velocities  $\dot{\theta}_1$  and  $\dot{\theta}_2$ , as shown in Figures 7(a) and 7(b), respectively. A small variation of steady-state energy was added to the initial conditions as  $\zeta = \mathcal{E}_0/100$ . The surface of the Poincaré map  $\mathcal{S}$  for Figures 6(a) and 6(b), in red, shows a quasiperiodic behavior. This behavior, demonstrated in Figure 6, expresses the dynamics of the manipulator with flexible links without the addition of the load at the end of the effector.

To analyse the system with the nonideal load coupled to the manipulator, the same dynamical analysis of

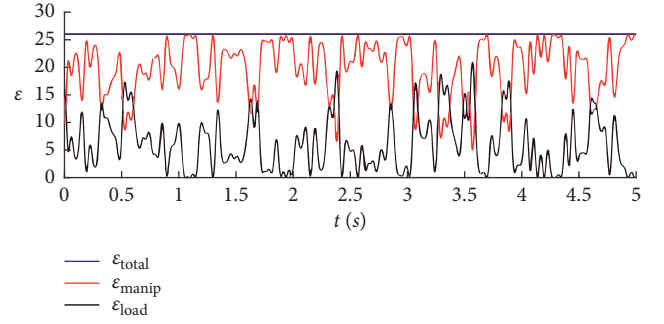


FIGURE 5: Kinetic energy exchange between load and manipulator with nonideal load.

TABLE 1: Parameters of the robot manipulator arm system.

Symbol	Description	Value	Unit
$R_a$	Motor armature resistance	1.5	$\Omega$
$L_a$	Motor inductance	0.0015	H
$k_t$	Motor torque constant	0.0185	Nm/A
$k_b$	Motor electromotive force	0.0185	V/rpm
$b_v$	Equivalent viscous friction	0.018	Nms
$\kappa$	Gear ratio	20.68	—
$\theta_M$	Angular position motor	$\eta\theta_M(t)$	rad
$\theta$	Angular position	—	rad
$\tau_f$	Total friction force	0.0021	Nm
$J$	Equivalent inertia load	—	$\text{kgm}^2$
$J_M$	Motor inertia	0.0185	—
$i$	Armature electrical current	—	A
$v$	Voltage armature motor	—	Volts
$\tau_s$	Cubic spring force	0.087	$\text{Nm}^3$
$k_s$	Flexibility of the transmission of the motor	350	$\text{Kg/s}^2$
$k_c$	Flexibility of the arm-load cable	150	Nms
$l_1$	Link 1 length	0.8	m
$l_2$	Link 2 length	0.8	m
$m_1$	Link 1 mass	0.4	kg
$m_2$	Link 2 mass	0.4	kg
$m_3$	Payload mass	0.6	kg
$\mathbf{x}$	State vector	—	—
$\mathbf{x}_d$	Setpoint vector	—	—
$\mathbf{e}$	Position error	—	—
$\mathbf{A}$	State matrix	—	—
$\mathbf{B}$	Input matrix	—	—
$\mathbf{Q}$	State weights matrix	—	—
$\mathbf{R}$	Input weights matrix	—	—
$\mathcal{CO}$	Controllability matrix	—	—

Figure 6 is carried out; however, the load dynamics is added. By setting the axes  $\theta_4$  and  $\theta_5$ , the energy  $\mathcal{E} = \mathcal{E}_0 + \zeta$  is defined, where  $\zeta = \mathcal{E}_0/100$ . Figure 7 presents the system dynamics with the nonideal load coupled to the end of the manipulator. These Figures 7(a) and 7(b) show the non-periodic orbits that represent the behavior of the system, since the phase plane crosses the surface of Poincaré in several different points. Such behavior, in the analysis of dynamic systems, can be classified with evidence of chaotic behavior; however, it is necessary to use another analytical tool to verify the chaos.

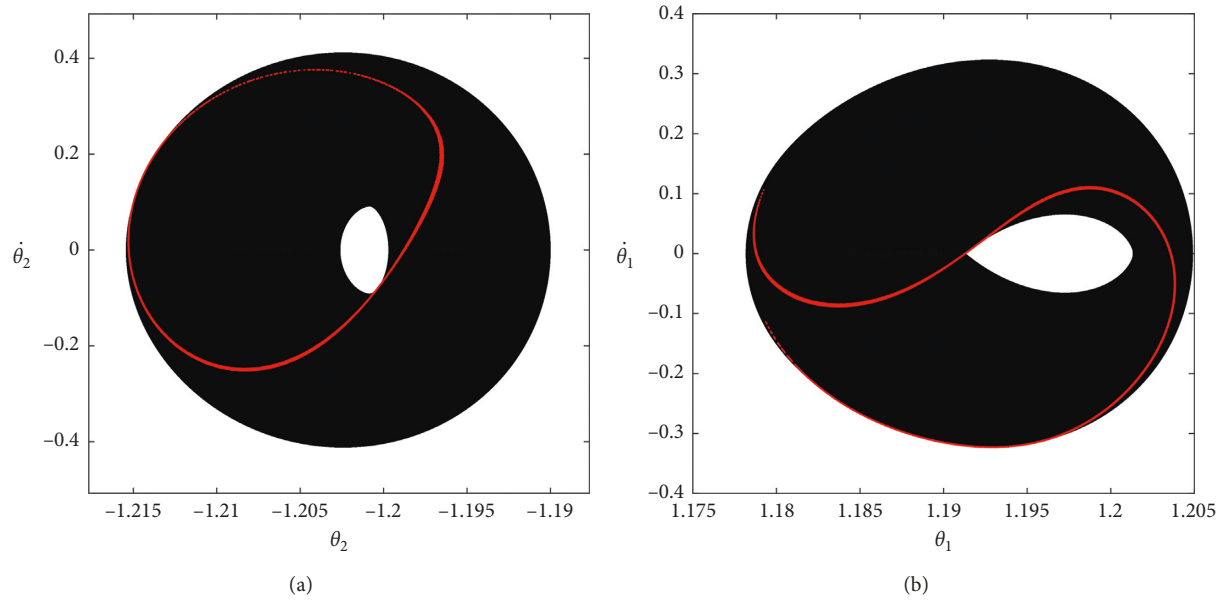


FIGURE 6: Phase planes (in black) and Poincaré Map (in red) for nonloaded-free system. (a) Poincaré section of  $\theta_1$  and (b) Poincaré section of  $\theta_2$ .

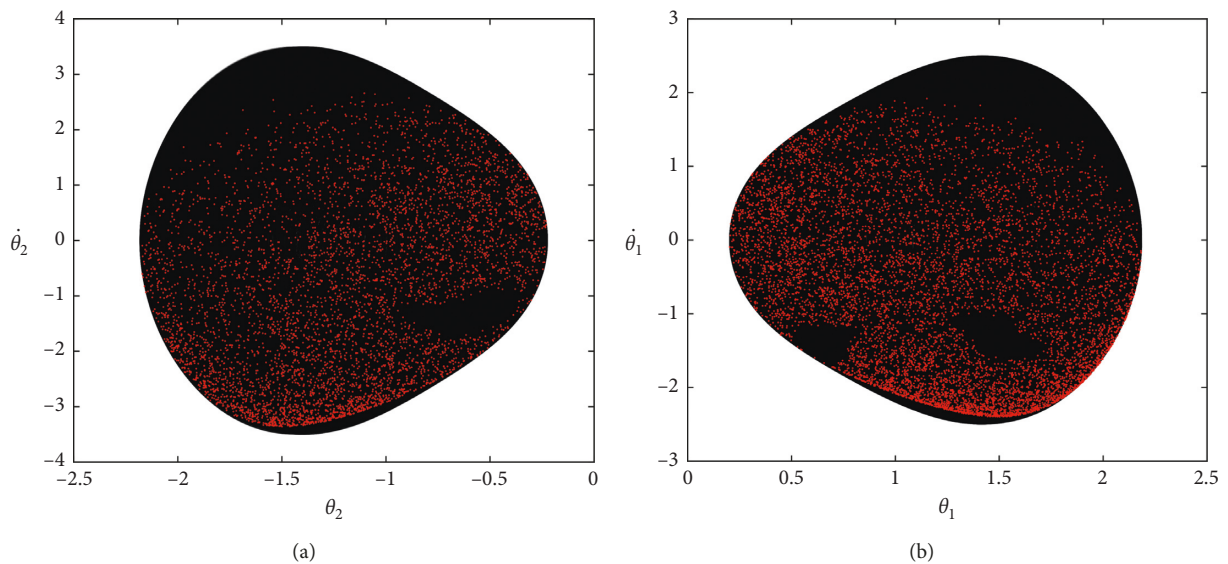


FIGURE 7: Phase planes (in black) and Poincaré map (in red) for nonideal loaded manipulator. (a) Poincaré section of  $\theta_1$  and (b) Poincaré section of  $\theta_2$ .

The Lyapunov exponent method consists of the analysis of the sensitivity of the initial conditions of a dynamical system being able to show if a system has periodic, quasiperiodic, or chaotic behavior. Applying this method to the model of manipulator with nonideal load coupled to its end, Figure 8 shows the three most relevant exponents. The system showed to be very sensitive to their initial conditions due to the existence of a positive exponent, which is  $\lambda_1 = 3.2$  in red. In addition, as there is at least one positive exponent, the behavior of the system is characterized as chaotic.

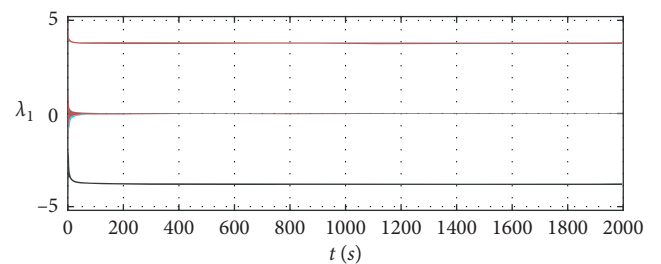


FIGURE 8: Three most relevant Lyapunov exponents to nonideal loaded manipulator.

Next, a control strategy is proposed to suppress the chaotic behavior.

#### 4. Control Strategy

The control strategy to be considered is the SDRE (state-dependent Riccati equation). The well-known SDRE controller has become very popular within the control community in the last decade, providing a very effective algorithm solution to synthesize nonlinear feedback controls by allowing nonlinearities in the states of the system in addition to offer great design flexibility through that of the dependent-state weighting matrices.

*4.1. Discrete Time SDRE Controller Design.* The control strategy proposed here is based on continuous time SDRE; however, in this actual application, it is necessary to incorporate the control into a digital device; thus, one should adjust the design to the DSDRE (discrete-time state-dependent Riccati equation) topology.

The first step is to define the error vector in which it should be minimized. In this work, typically, the error vector is composed of the states related to a new coordinate in which the manipulator must reach; thus, the error equation should be defined as

$$\mathbf{e}(t) = \mathbf{x}(t) - \mathbf{x}_d(t), \quad (18)$$

where  $\mathbf{e}(t)$  is the error vector,  $\mathbf{x}_d(t)$  represents the desired coordinate, and  $\mathbf{x}$  is obtained by finding the static equilibrium point for the positioning coordinates.

The optimal control problem for the system with coefficients of the state matrix and infinite horizon condition can be formulated as a function of the new error coordinates, as in the following equation:

$$J_k = \frac{1}{2} \int_0^{\infty} [\mathbf{e}(t)^T \mathbf{Q} \mathbf{e}(t) + \mathbf{u}(t)^T \mathbf{R} \mathbf{u}(t)] dt. \quad (19)$$

The solution of the optimal control problem is obtained by the Riccati equation, given by the following equation:

$$\mathbf{A}(\mathbf{e}(t), t)^T \mathbf{P} + \mathbf{P} \mathbf{A}(\mathbf{e}(t), t) - \mathbf{P} \mathbf{B} \mathbf{R}^{-1} \mathbf{B}^T \mathbf{P} + \mathbf{Q} = 0. \quad (20)$$

Although the solution of equation (20) provides an optimal control solution, in the SDRE control, this solution is presented as suboptimal because each interaction recalculates the local optimal value for the control, based on the error state arrays  $\mathbf{A}(\mathbf{e}(t), t)$  and  $\mathbf{B}$ .

The matrices  $\mathbf{Q}$  and  $\mathbf{R}$  are semidefinite and positive,  $\mathbf{Q} > 0$ ,  $\mathbf{R} > 0$ , guaranteeing that the system is asymptotically stable [26]. Therefore, the dynamic equation of the error can be rewritten as follows:

$$\dot{\mathbf{e}}(t) = [\mathbf{A}(\mathbf{e}(t), t) - \mathbf{B} \mathbf{K}(\mathbf{e}(t), t)] \mathbf{x}(t). \quad (21)$$

The matrix of controller gains is given by  $\mathbf{K}(\mathbf{e}(t), t)$ , defined by the following equation:

$$\mathbf{K}(\mathbf{e}(t), t) = \mathbf{R}^{-1} \mathbf{B}^T \mathbf{P}. \quad (22)$$

Besides, the choosing of the parameter of performance matrices  $\mathbf{Q}$  and  $\mathbf{R}$  is an important factor to ensure optimality, a dynamic system does not always have full controllability of the states; in this way, it should be verified the controllability matrix for each interaction, according to the controllability theorem.

A dynamic system such as equation (21) is completely controllable if and only if the controllability matrix station is equal to  $n$ , which is defined by

$$\mathcal{C} \mathcal{C} = \text{rank}([\mathbf{B} \ \mathbf{A}(\mathbf{x}(t), t) \mathbf{B} \ \dots \ \mathbf{A}^{n-1}(\mathbf{x}(t), t) \mathbf{B}]), \quad (23)$$

where  $n$  represents the dimension of the state matrix  $\mathbf{A}(\mathbf{x}(t), t)^{n \times n}$ .

However, the proposal presented above applies to continuous time ( $t$ ); thus, the controller must be adapted to be shipped in a digital device.

In a digital device, the time relationship is limited to the physical characteristics of a microcontrollable device; for example, the conversion time from the analogue to the digital system can set the minimum time of operation of the variables for a real-time representation. At this discrete time unit, the denomination of sampling time is given by ( $T_s$ ).

According to [15], since there is a  $\mathbf{u}(t)$  for  $kT_s \leq t < (k+1)T_s$ , where  $k = 0, 1, 2, N-1$ , it can be substituted to  $\mathbf{u}(t) \approx \mathbf{u}(kT_s)$ . In this way, the discretization of a system of dynamic equations can be rewritten by

$$\mathbf{x}_{k+1} = e^{\mathbf{A}T_s} \mathbf{x}_k + \int_0^{T_s} e^{\mathbf{A}\gamma} \mathbf{B} \mathbf{u}_k d\gamma, \quad (24)$$

with  $t = kT_s$ , where  $\gamma = T_s - t$ , consequently, the transformation matrix for discretization of the system is given by the following equation:

$$\begin{aligned} \mathbf{A}_k &= e^{\mathbf{A}T_s}, \\ \mathbf{B}_k &= \left( \int_0^{T_s} e^{\mathbf{A}\gamma} d\gamma \right) \mathbf{B}. \end{aligned} \quad (25)$$

For  $T_s$  significantly small in reaction to the dynamics of the system, it is obtained the discretized system matrix through the first order of the Taylor series, given as

$$\begin{aligned} \mathbf{A}_k &\approx \mathbf{A}T_s + \mathbf{I}, \\ \mathbf{B}_k &\approx \mathbf{B}T_s, \end{aligned} \quad (26)$$

where  $\mathbf{I}$  is an identity matrix.

Once the matrices of the discretized system are defined, it is possible to state the minimization function of the controller error for discrete time, which is

$$J_k = \frac{1}{2} \sum_{k=0}^{N-1} [\mathbf{e}_k^T \mathbf{Q} \mathbf{e}_k + \mathbf{u}_k^T \mathbf{R} \mathbf{u}_k]. \quad (27)$$

The solution of equation (27) can be obtained through the DARE (algebraic solution of the Riccati discrete equation), which is demonstrated by the following equation:

$$\mathbf{P}_k = \mathbf{Q} + \mathbf{A}_k^T \mathbf{P}_{k-1} \mathbf{A}_k - \mathbf{A}_k^T \mathbf{P}_{k-1} \mathbf{B}_k [\mathbf{R} + \mathbf{B}_k^T \mathbf{P}_{k-1} \mathbf{B}_k]^{-1} \mathbf{B}_k^T \mathbf{P}_{k-1} \mathbf{A}_k. \quad (28)$$

The equation of controller gains  $\mathbf{K}_k$  for each discrete time interaction  $k$  is then defined by the following equation:

$$\mathbf{K}_k = \mathbf{R}^{-1} \mathbf{B}_k^T (\mathbf{A}_k^T)^{-1} [\mathbf{P}_k - \mathbf{Q}]. \quad (29)$$

For a better visualization of the controller calculation steps, the control Algorithm 1 is shown. The Algorithm 1 recalculates the control vector  $\mathbf{K}_k$  at each interval of  $T_s$ , obtaining the local optimal value of the system.

Considering the dynamics of the manipulator, the DC motor is coupled in the axis  $\theta_M = [\theta_4 \ \theta_5]^T$ , giving the equations of motion of the controlled system denoted by the following equation:

$$\mathbf{M}(\theta, \ell) \begin{Bmatrix} \ddot{\theta} \\ \ddot{\ell} \\ \ddot{\theta}_M \\ \ddot{i}_M \end{Bmatrix} + \mathbf{C}(\dot{\theta}, \dot{\ell}, \theta, \ell) \begin{Bmatrix} \dot{\theta} \\ \dot{\ell} \\ \dot{\theta}_M \\ \dot{i}_M \end{Bmatrix} + \mathbf{K}(\theta, \ell, \theta_M, i_M) \begin{Bmatrix} \theta \\ \ell \\ \theta_M \\ i_M \end{Bmatrix} + \mathbf{G}(\theta) = \mathbf{U}(v). \quad (30)$$

$$\begin{Bmatrix} \ddot{\theta} \\ \ddot{\ell} \\ \ddot{\theta}_M \\ \ddot{i}_M \end{Bmatrix} = \mathbf{M}(\theta, \ell)^{-1} \left( -\mathbf{C}(\dot{\theta}, \dot{\ell}, \theta, \ell) \begin{Bmatrix} \dot{\theta} \\ \dot{\ell} \\ \dot{\theta}_M \\ \dot{i}_M \end{Bmatrix} - \mathbf{K}(\theta, \ell, \theta_M, i_M) \begin{Bmatrix} \theta \\ \ell \\ \theta_M \\ i_M \end{Bmatrix} - \mathbf{G}(\theta) + \mathbf{U}(v) \right). \quad (31)$$

After isolating the accelerations, the system is transformed in state-space notation, being that  $\mathbf{x}$  is  $\mathbf{x} = [\theta_1 \ \dot{\theta}_1 \ \theta_2 \ \dot{\theta}_2 \ \theta_3 \ \dot{\theta}_3 \ \ell \ \dot{\ell} \ \theta_{M_1} \ \dot{\theta}_{M_1} \ \theta_{M_2} \ \dot{\theta}_{M_2} \ i_{M_1} \ \dot{i}_{M_1} \ i_{M_2} \ \dot{i}_{M_2}]$ , whose system in state-space notation in the matrix form is given by the following equation:

$$\dot{\mathbf{x}}(t) = \mathbf{A}(\mathbf{x}(t), t) \mathbf{x}(t) + \mathbf{B} \mathbf{u}(t) + \mathbf{G}(\mathbf{x}), \quad (32)$$

where  $\mathbf{A}$  is the state matrix,  $\mathbf{B}$  is the control matrix, and  $\mathbf{G}(\mathbf{x})$  is the gravitational change. The controller design matrices are presented by the following equation:

$$\begin{aligned} \mathbf{Q} &= 100 \cdot \mathbf{I}^{10 \times 10}, \\ \mathbf{R} &= 0.001 \cdot \mathbf{I}^{2 \times 2}, \end{aligned} \quad (33)$$

where  $\mathbf{I}$  is the identity matrix.

The closed-loop control represented in block diagrams is illustrated in Figure 9.

Defining the positions of the desired coordinates as  $\mathbf{x}_d = [\theta_1 \ \theta_2]$ , where  $\theta_1 = \pi/2$  rad ( $90^\circ$ ) and  $\theta_2 = 0$  rad, the results of the control can be observed in Figure 9. It should be noted that the goal of  $\mathbf{x}_d$  refers to the final position of the axes  $\theta_1$  and  $\theta_2$ , where the inclusion of the nonideal load  $\ell$  has a disturbing effect on the system.

Figure 10 shows  $e_1 = \theta_1 - x_{d_1}$  and  $e_2 = \theta_2 - x_{d_2}$ . It can be seen that response of Figure 10 has a steady-state error. The disturbance oscillation  $\ell$  was absorbed by the manipulator.

```

Data: Continuous time variables  $\mathbf{A}, \mathbf{B}, \mathbf{Q}, \mathbf{R}, \mathbf{P}_{k-1}$ 
Results:  $\mathbf{K}_k$  control vector
Initiating;
Read the arrays  $\mathbf{A}, \mathbf{B}, \mathbf{Q}, \mathbf{R}, \mathbf{P}_{k-1}$ ;
 $\mathcal{C} = \text{rank}([\mathbf{B} \ \mathbf{A}(\mathbf{x}(t), t) \mathbf{B} \dots \mathbf{A}^{n-1}(\mathbf{x}(t), t) \mathbf{B}])$ 
if  $\mathcal{C} = n$  then
  while  $|\det(\mathbf{P}_{k-1}) - \det(\mathbf{P}_k)| < 0.01$  do
    Calc Matrix  $\mathbf{A}_k$  and  $\mathbf{B}_k$ ;
    Calc  $\mathbf{P}_k$  in equation (28);
    Find the controller gains;
     $\mathbf{K}_k = \mathbf{R}^{-1} \mathbf{B}_k^T (\mathbf{A}_k^T)^{-1} [\mathbf{P}_k - \mathbf{Q}]$ 
  end
else
   $\mathbf{K}_k = \mathbf{K}_{k-1}$ 
end

```

ALGORITHM 1: Calculation of control vector  $\mathbf{K}_k$  for control DSDRE.

For the application of state-space control, it is necessary to isolate the system acceleration vector of equation (30) described by the following equation:

## 5. Magnetorheological Actuator

The MR fluids belong to a family of rheological materials that undergo phase change under the application of magnetic fields. Typically, MR fluids are composed of ferromagnetic or soft paramagnetic particles ( $0.03$  to  $10 \mu\text{m}$ ) dispersed in a carrier fluid. Due to design issues, magnetizable particles must have low levels of magnetic coercivity, and then, various types of materials have been applied to coat the ER (electrorheology) fluid [27] with ceramics and metal alloys.

The dynamic behavior of the MR fluids, from the theory of fluid mechanics, shows that with the absence of a magnetic field on the fluid, it is classified as a Newtonian fluid, whereas when exposed to a magnetic field exhibits Bingham [28] viscoelastic behavior, as represented in Figure 11. The electromagnetic field is typically generated by electric coils.

The equation that defines the behavior of a Bingham fluid is given by equation (34):

$$\tau_c = \tau_y(\cdot) + \eta \frac{dv}{dz}, \quad \tau_c > \tau_y, \quad (34)$$

where  $\tau_c$  represents the shear stress,  $\eta$  is the Newtonian viscosity coefficient,  $\gamma$  is the shear rate,  $\tau_y$  is the stress related to the dynamic behavior of the fluid MR, and  $dv/dz$  is the velocity gradient in the direction of the magnetic field.

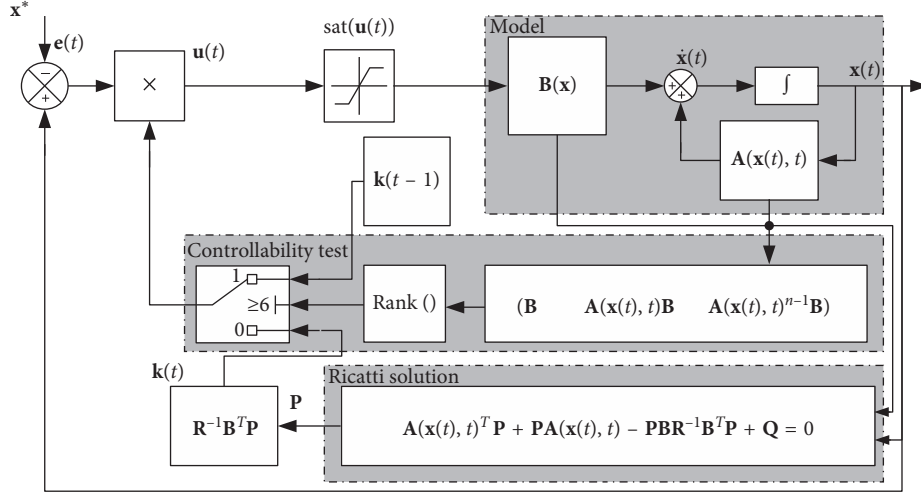


FIGURE 9: Block diagram of the system with control applied to the DC motor.

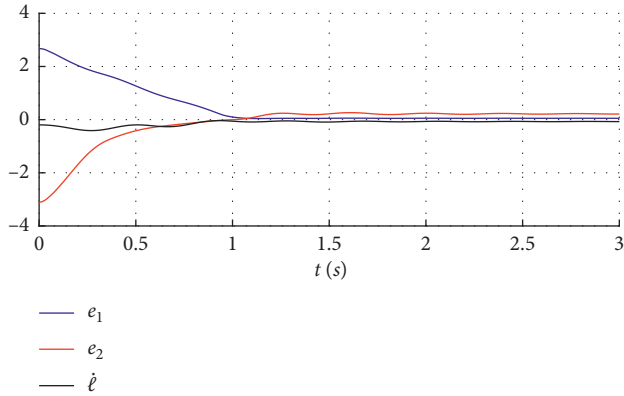


FIGURE 10: Positioning error response for nonideal loading manipulator with DC motor.

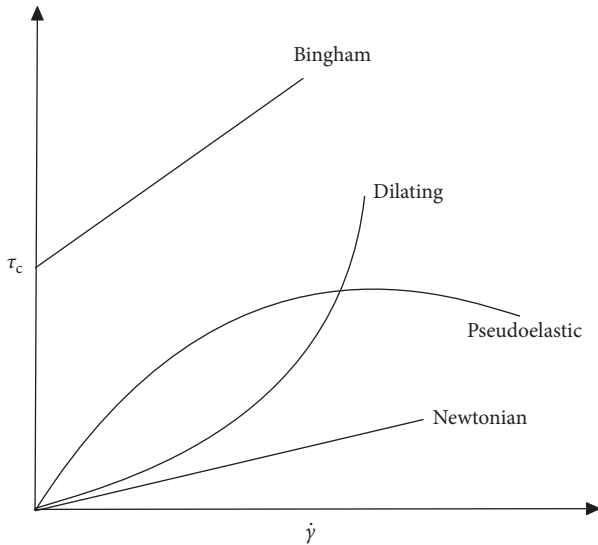


FIGURE 11: Fluid behavior.

As previously mentioned, when a magnetic field is applied in the fluid, the shear stress ratio can change; hence, the function  $\tau_y$  has a dependence on the intensity of the magnetic field, defined by  $H$ . The multidisc composite MR brake is adopted here, such approach is due to the lack of several discs increasing the contact region with the oil, allowing the reductions of spacing  $l_f$ .

Therefore, equation (34) is rewritten as equation (35), considering the magnetic field  $H$  and the radius  $r$  of the circumference of the disk:

$$\tau_c = \tau_y(H) + \eta \dot{\gamma}(r), \quad \text{where } \dot{\gamma}(r) = \frac{\omega r}{l_f}, \quad (35)$$

where the term  $\omega$  represents the speed of rotation of the disk.

The variation of torque produced by a circumferential element of the rotational brake of the MR of radius  $r$  is given by the following equation:

$$dT_{MR} = 2\pi r^2 \tau_c dr. \quad (36)$$

The geometric relation of  $r$  is given by the relation  $r = R_2 - R_1$ . In this way, it is possible to integrate equation (35) as a function of the circle radius of the disk, according to the following equation:

$$\begin{aligned} T_{MR} &= 2N \int_{R_1}^{R_2} 2\pi \left( \tau_y(H) r^2 + \eta \frac{\omega r^3}{l_f} \right) dr \\ &= 4N\pi \left( \frac{\tau_y(H) (R_2^3 - R_1^3)}{3} + \frac{\eta \omega (R_2^4 - R_1^4)}{4l_f} \right), \end{aligned} \quad (37)$$

where  $N$  represents the number of disks in the engine.

The above equations present the dynamics related to the MR fluid mechanics; however, for this work, the hybrid

actuator composition will be considered, being that the MR actuator aims at damping undesired vibrations in the robotic manipulator, as well as the coupling of the motor for positioning of the manipulator.

The equation that couples the MR actuator to the system is denoted by the following equation:

$$\begin{aligned}\ddot{\theta}_{MR} &= J_{eq}^{-1} (k_t i - b\omega - \tau_s(\theta, \theta_M) - T_{MR}) \\ &= J_{eq}^{-1} \left[ k_t i - \left( b + 4N\pi \frac{\eta(R_2^4 - R_1^4)}{4l_f} \right) \omega \right. \\ &\quad \left. - 4N\pi \left( \frac{\tau_y(H)(R_2^3 - R_1^3)}{3} \right) - \tau_s(\theta, \theta_M) \right].\end{aligned}\quad (38)$$

At last, finalizing equation (38), it is necessary to define the relation between  $\tau_y$  and the magnetic field generated by the coils of the MR actuator. In this context, there are two fundamental laws of magnetic field and flux: Ampere's law and Gauss' law. This deduction is made typically for a MR project, where it can be related to the magnetic field lines that pass through the MR fluid; however, the described curve of authors in [29] was adopted, where the fluid dynamics is found by the following equation:

$$\tau_y = \alpha H^\beta, \quad (39)$$

where  $\alpha$  and  $\beta$  are obtained from the experimental curve of the MR fluid.

Then, equation (39) is rewritten, denoted by the following equation:

$$\begin{pmatrix} \ddot{\theta} \\ \ddot{\ell} \\ \ddot{\theta}_{MR} \\ \ddot{i}_M \end{pmatrix} = \mathbf{M}(\theta, \ell)^{-1} \left( -\mathbf{C}(\dot{\theta}, \dot{\ell}, \theta, \ell) \begin{pmatrix} \dot{\theta} \\ \dot{\ell} \\ \dot{\theta}_{MR} \\ \dot{i}_M \end{pmatrix} - \mathbf{K}(\theta, \ell, \theta_{MR}, i_M) - \mathbf{G}(\theta) + \mathbf{U}(v, T_{MR}) \right). \quad (42)$$

In this way, after isolating the accelerations, the system is transformed state-space form, being that  $\mathbf{x} = [\theta_1 \ \dot{\theta}_1 \ \theta_2 \ \dot{\theta}_2 \ \theta_3 \ \dot{\theta}_3 \ \ell \ \dot{\ell} \ \theta_{MR_1} \ \dot{\theta}_{MR_1} \ \theta_{MR_2} \ \dot{\theta}_{MR_2} \ \theta_{MR_3} \ \dot{\theta}_{MR_3} \ i_{M_1} \ \dot{i}_{M_1} \ i_{M_2} \ \dot{i}_{M_2}]$ . The state-space system in the matrix form is given by equation (43), where  $\mathbf{A}$  is the state matrix,  $\mathbf{B}$  is the control matrix, and  $\mathbf{G}(\mathbf{x})$  is the gravitational change:

$$\dot{\mathbf{x}}(t) = \mathbf{A}(\mathbf{x}(t), t)\mathbf{x}(t) + \mathbf{B}\mathbf{u}(t) + \mathbf{G}(\mathbf{x}). \quad (43)$$

The controller design matrices are presented by the following equation:

$$\begin{aligned}\mathbf{Q} &= 100 \cdot \mathbf{I}^{10 \times 10}, \\ \mathbf{R} &= 0.001 \cdot \mathbf{I}^{4 \times 4},\end{aligned}\quad (44)$$

where  $\mathbf{I}$  is the identity matrix.

The closed-loop control for the MR brake represented in block diagrams is illustrated by Figure 12.

$$\begin{aligned}\ddot{\theta}_{MR} &= J_{eq}^{-1} \left[ k_t i - \left( b + 4N\pi \frac{\eta(R_2^4 - R_1^4)}{4l_f} \right) \omega \right. \\ &\quad \left. - 4N\pi \alpha \left( \frac{R_2^3 - R_1^3}{3} \right) H^\beta - \tau_s(\theta, \theta_M) \right]\end{aligned}\quad (40)$$

$$\frac{d}{dt} i_M = L_a^{-1} [-R_a i - k_b \omega + v].$$

The MR actuator has two control inputs:  $v(t)$ , the motor voltage for positioning, and  $H(t)$ , for control of the viscosity component in order to eliminate the vibration of the system.

As a proposal to improve the manipulator for nonideal loading, the model where the MR actuator is coupled is presented, according to the following equation:

$$\begin{aligned}\mathbf{M}(\theta, \ell) \begin{pmatrix} \ddot{\theta} \\ \ddot{\ell} \\ \ddot{\theta}_{MR} \\ \ddot{i}_M \end{pmatrix} + \mathbf{C}(\dot{\theta}, \dot{\ell}, \theta, \ell) \begin{pmatrix} \dot{\theta} \\ \dot{\ell} \\ \dot{\theta}_{MR} \\ \dot{i}_M \end{pmatrix} \\ + \mathbf{K}(\theta, \ell, \theta_{MR}, i_M) + \mathbf{G}(\theta) = \mathbf{U}(v, T_{MR}).\end{aligned}\quad (41)$$

For the application of state-space control, it is necessary to isolate the system acceleration vector, equation (41), becoming

The values for the desired trajectory  $\mathbf{x}_d$  are maintained as in the previous case. Likewise, the goal of  $\mathbf{x}_d$  refers to the final position of the axes  $\theta_1$  and  $\theta_2$ , where the inclusion of the nonideal load  $\ell$  is presented as a perturbation effect to the system. Then, the system response is shown by Figure 13.

It can be seen that the MR utilization caused the system to not oscillate and caused less error in the steady-state regime, as Figure 14.

In Figure 15, the robot displacement trajectory in 5(s) can be seen, considering the robot displacement trajectory by control without and with MR brake.

Figure 16 shows the DC motor control input.

Figure 17 shows the control torque to joints.

The current curves to be applied to the MR can be seen in Figure 18.

As can be observed in the simulation results, with the use of the MR brake, it was possible to reduce the oscillations of the suspended mass.

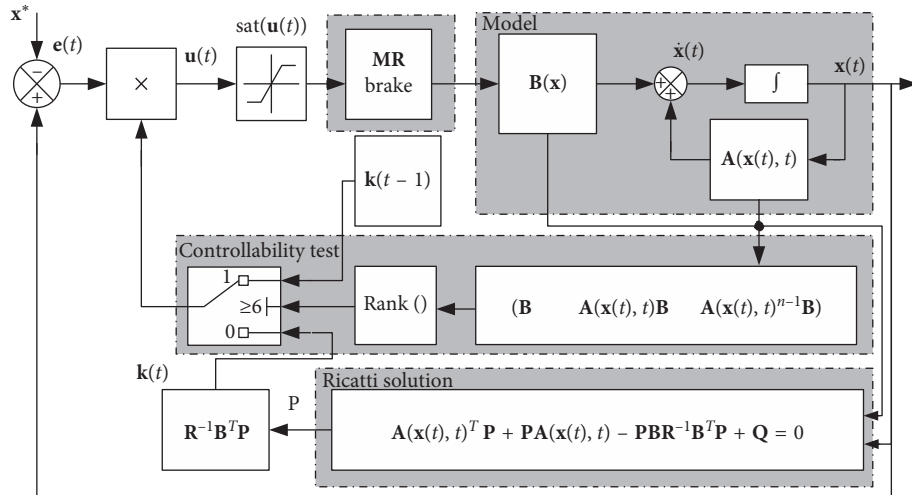


FIGURE 12: Block diagram of the system with control applied to the DC motor and MR brake.

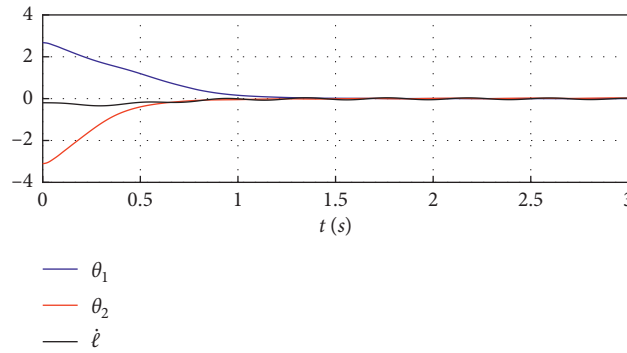


FIGURE 13: Positioning error response for nonideal loading manipulator with DC motor and MR brake.

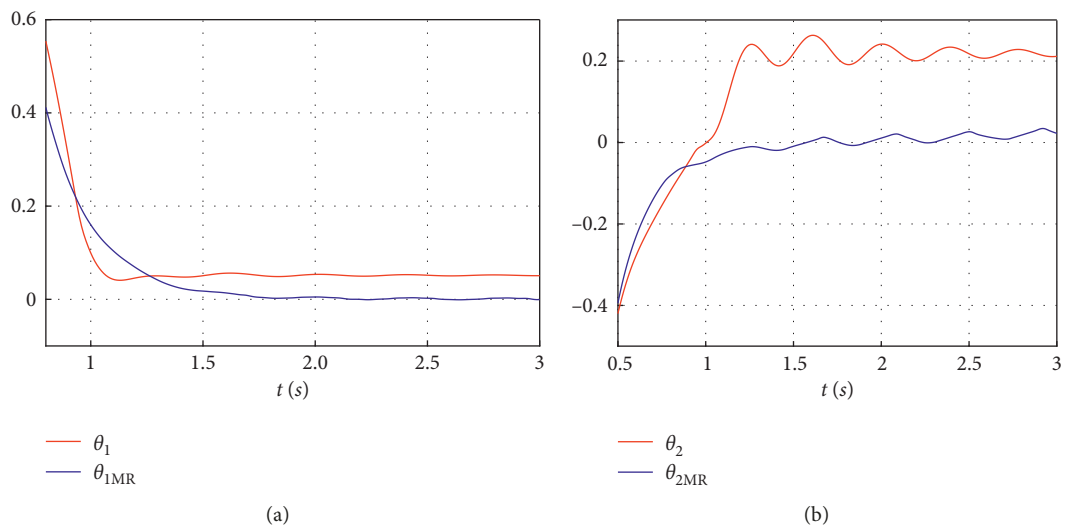


FIGURE 14: Comparison between the results of the manipulator with motor (in red) and MR coupling (in blue).

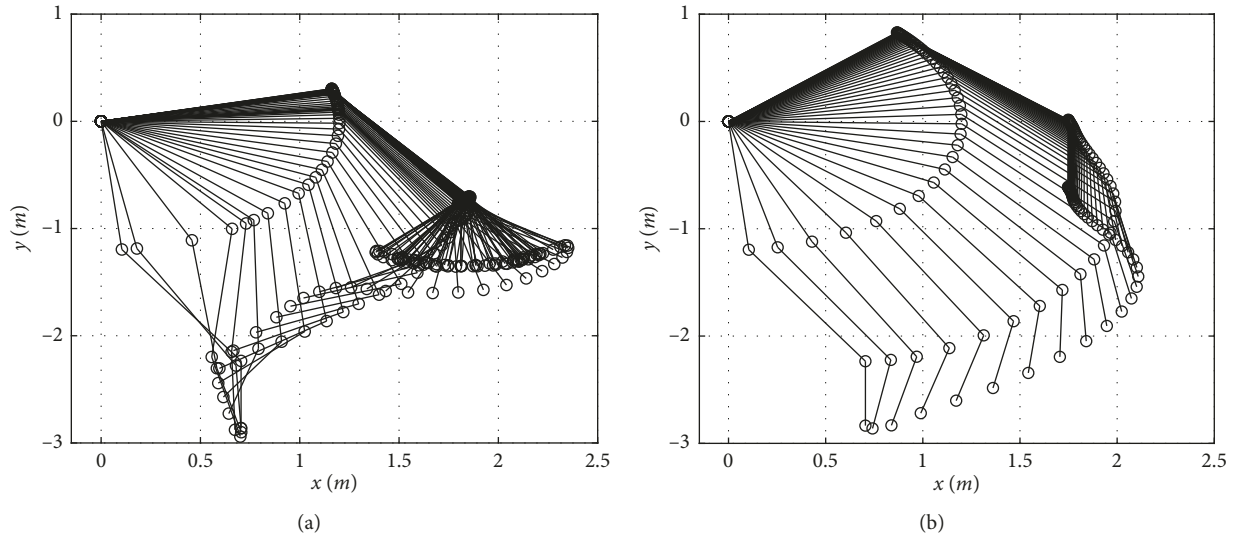


FIGURE 15: Robot displacement trajectory (5s). Robot displacement trajectory by control (a) without MR and (b) with MR.

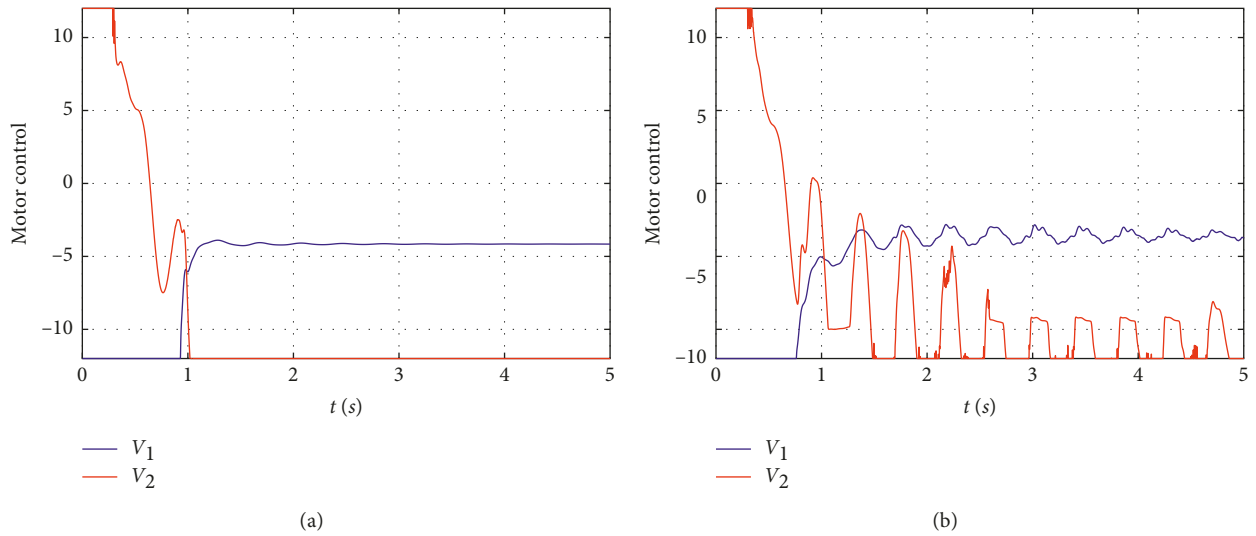


FIGURE 16: Voltage control of motor for control (a) without MR brake and (b) with MR brake.

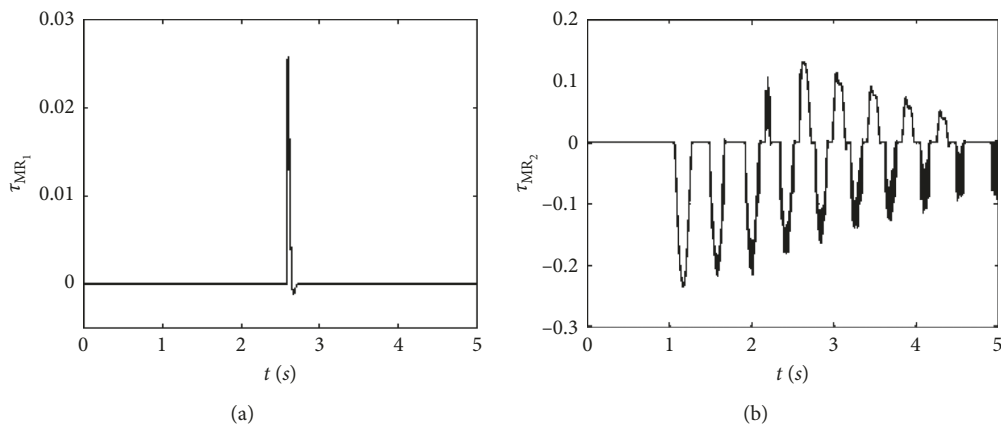


FIGURE 17: (a) Torque control MR brake joint one. (b) Torque control MR brake joint two.

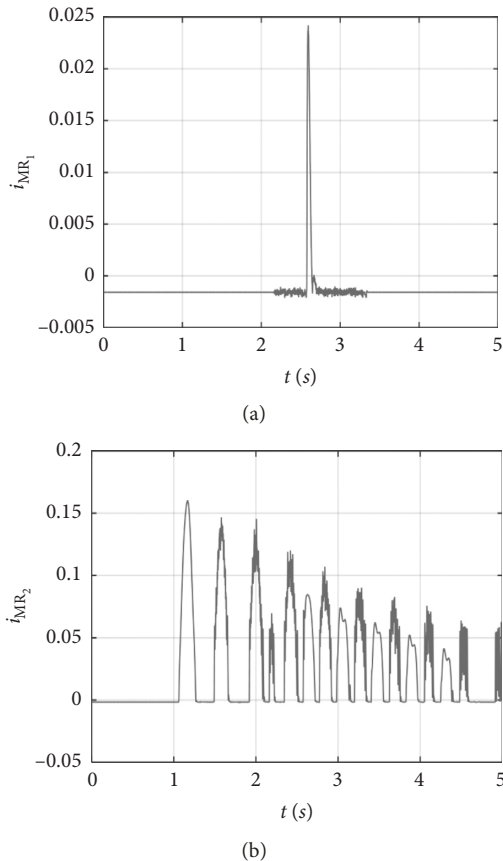


FIGURE 18: Estimative current to control MR brake torque in (a) joint one and (b) joint two.

## 6. Conclusions

This work presented the efficiency of the SDRE controller technique using a DC motor and the DC motor with a MR brake coupling to control a robot manipulator of flexible links and joints with a free load at its end.

Using only the DC motor, it was possible to control the system leading the manipulator arms to the desired trajectory, and the error was very small. Using the DC motor and MR brake, the arms also led to the desired trajectory; however, the error was minimized almost to zero, showing that using multiple actuators improve the control performance and minimize the interference of external disturbances.

## Data Availability

The authors declare that data are available for researchers upon request to the corresponding author.

## Conflicts of Interest

The authors declare that they have no conflicts of interest.

## Acknowledgments

The authors acknowledge financial support by the CNPq, CAPES, and FA, all Brazilian research funding agencies. In

addition, the authors thank the organizing committee of the International Mechanical Engineering Congress and Exposition (ASME 2016), where part of this work was presented.

## References

- [1] M. Avraam, M. Horodincu, I. Romanescu, and A. Preumont, "Computer controlled rotational MR-brake for wrist rehabilitation device," *Journal of Intelligent Material Systems and Structures*, vol. 21, no. 15, pp. 1543–1557, 2010.
- [2] J. Z. Chen and W. H. Liao, "Design, testing and control of a magnetorheological actuator for assistive knee braces," *Smart Materials and Structures*, vol. 19, no. 3, article 035029, 2010.
- [3] M. M. Fateh, "Robust control of flexible-joint robots using voltage control strategy," *Nonlinear Dynamics*, vol. 67, no. 2, pp. 1525–1537, 2012.
- [4] J. Huang, J. Q. Zhang, Y. Yang, and Y. Q. Wei, "Analysis and design of a cylindrical magneto-rheological fluid brake," *Journal of Materials Processing Technology*, vol. 129, no. 1–3, pp. 559–562, 2002.
- [5] R. Jablonski, M. Turkowski, and R. Szewczyk, *Recent Advances in Mechatronics*, Springer Science and Business Media, Berlin, Germany, 2007.
- [6] B. Siciliano and O. Khatib, *Springer Handbook of Robotics*, Springer-Verlag Berlin Heidelberg, Berlin, Germany, 2016.
- [7] M. Kalyoncu, "Mathematical modelling and dynamic response of a multi-straight-line path tracing flexible robot manipulator with rotating-prismatic joint," *Applied Mathematical Modelling*, vol. 32, no. 6, pp. 1087–1098, 2008.
- [8] A. Shawky, D. Zydek, Y. Z. Elhalwagy, and A. Ordys, "Modeling and nonlinear control of a flexible-link manipulator," *Applied Mathematical Modelling*, vol. 37, no. 23, pp. 9591–9602, 2013.
- [9] J. J. Lima, A. M. Tusset, F. C. Janzen et al., "SDRE applied to position and vibration control of a robot manipulator with a flexible link," *Journal of Theoretical and Applied Mechanics*, vol. 54, no. 4, pp. 1067–1078, 2016.
- [10] A. Molter, O. A. A. da Silveira, J. S. O. Fonseca, and V. Bottega, "Simultaneous piezoelectric actuator and sensor placement optimization and control design of manipulators with flexible links using SDRE method," *Mathematical Problems in Engineering*, vol. 2010, Article ID 362437, 23 pages, 2010.
- [11] A. M. Tusset, J. M. Balthazar, D. G. Bassinello, B. R. Pontes Jr., and J. L. P. Felix, "Statements on chaos control designs, including a fractional order dynamical system, applied to a "MEMS" comb-drive actuator," *Nonlinear Dynamics*, vol. 69, no. 4, pp. 1837–1857, 2012.
- [12] A. M. Tusset, J. M. Balthazar, and J. L. P. Felix, "On elimination of chaotic behavior in a non-ideal portal frame structural system, using both passive and active controls," *Journal of Vibration and Control*, vol. 19, no. 6, pp. 803–813, 2013.
- [13] A. M. Tusset, A. M. Bueno, C. B. Nascimento, K. M. dos Santos, and J. M. Balthazar, "Nonlinear state estimation and control for chaos suppression in MEMS resonator," *Shock and Vibration*, vol. 20, no. 4, pp. 749–761, 2013.
- [14] J. J. de Lima, A. M. Tusset, F. C. Janzen et al., "Nonlinear state estimation and control applied to a manipulator robotic including drive motor," *Mathematics in Engineering, Science and Aerospace (MESA)*, vol. 5, no. 4, 2014.
- [15] A. Fenili and J. M. Balthazar, "The rigid-flexible nonlinear robotic manipulator: modeling and control," *Communications*

- in Nonlinear Science and Numerical Simulation*, vol. 16, no. 5, pp. 2332–2341, 2011.
- [16] M. Innocenti, F. Baralli, F. Salotti, and A. Caiti, “Manipulator path control using SDRE,” in *Proceedings of American Control Conference*, pp. 3348–3352, San Francisco, CA, USA, June–July 2010.
- [17] M. H. Korayem, M. Irani, and S. R. Nekoo, “Analysis of manipulators using SDRE: a closed loop nonlinear optimal control approach,” *Scientia Iranica. Transaction B, Mechanical Engineering*, vol. 17, no. 6, p. 456, 2010.
- [18] M. H. Korayem, M. Irani, and S. R. Nekoo, “Load maximization of flexible joint mechanical manipulator using nonlinear optimal controller,” *Acta Astronautica*, vol. 69, no. 7–8, pp. 458–469, 2011.
- [19] M. H. Korayem and S. R. Nekoo, “Nonlinear optimal control via finite time horizon state-dependent Riccati equation,” in *Proceedings of 2014 Second RSI/ISM International Conference on Robotics and Mechatronics (ICRoM)*, pp. 878–883, IEEE, Tehran, Iran, October 2014.
- [20] M. H. Korayem and S. R. Nekoo, “State-dependent differential Riccati equation to track control of time-varying systems with state and control nonlinearities,” *ISA transactions*, vol. 57, pp. 117–135, 2015.
- [21] M. H. Korayem and S. R. Nekoo, “Finite-time state-dependent Riccati equation for time-varying nonaffine systems: rigid and flexible joint manipulator control,” *ISA transactions*, vol. 54, pp. 125–144, 2015.
- [22] S. R. Nekoo, “Nonlinear closed loop optimal control: a modified state-dependent Riccati equation,” *ISA transactions*, vol. 52, no. 2, pp. 285–290, 2013.
- [23] M. Xin, S. N. Balakrishnan, and Z. Huang, “Robust state dependent Riccati equation based robot manipulator control,” in *Proceedings of Proceedings of the 2001 IEEE International Conference on Control Applications (CCA’01)*, pp. 369–374, IEEE, Mexico City, Mexico, September 2001.
- [24] A. M. Tusset, F. C. Janzen, V. Piccirillo et al., “On nonlinear dynamics of a parametrically excited pendulum using both active control and passive rotational (MR) damper,” *Journal of Vibration and Control*, vol. 24, no. 9, pp. 1587–1599, 2018.
- [25] J. J. Lima, R. T. Rocha, F. C. Janzen, A. M. Tusset, D. G. Bassinello, and J. M. Balthazar, “Position control of a manipulator robotic arm considering flexible joints driven by a DC motor and a controlled torque by a MR-brake,” in *ASME 2016 International Mechanical Engineering Congress and Exposition*, Vol. 4, Dynamics, Vibration, and Control, Phoenix, AZ, USA, 2016.
- [26] H. Ishii and B. A. Francis, *Limited Data Rate in Control Systems with Networks*, Springer Science and Business Media, Vol. 275, Springer Science and Business Media, Berlin, Germany, 2002.
- [27] R. Stanway, J. L. Sproston, and A. K. El-Wahed, “Applications of electro-rheological fluids in vibration control: a survey,” *Smart Materials and Structures*, vol. 5, no. 4, p. 464, 1996.
- [28] Q. H. Nguyen and S. B. Choi, “Optimal design of MR shock absorber and application to vehicle suspension,” *Smart materials and Structures*, vol. 18, no. 3, article 035012, 2009.
- [29] I. H. Shames and F. A. Cozzarelli, *Elastic and Inelastic Stress Analysis*, CRC Press–Taylor and Francis Group LLC, Boca Raton, FL, USA, 1997.



**Hindawi**

Submit your manuscripts at  
[www.hindawi.com](http://www.hindawi.com)

